Design and Analysis of Sliding Mode Controller Under Approximate Hysteresis Compensation

Mohamed Edardar, Xiaobo Tan, *Senior Member, IEEE*, and Hassan K. Khalil, *Fellow, IEEE*

***Abstract*— A sliding mode controller (SMC) is proposed for a class of systems comprising a hysteresis operator preceding a linear system with an all-pole transfer function. The hysteresis operator is modeled with uncertain piecewise linear characteristics, and a nominal inverse operator is included to mitigate the hysteresis effect. A classical SMC design typically uses a constant coefficient in the switching component, which is tuned via trial-and-error. In this paper, a state- and time-dependent coefficient is proposed based on the derived inversion error, which eliminates the need for parameter tuning and ensures the convergence of the sliding surface to the boundary layer without compactness assumptions. In addition, singular perturbation is used to analyze the system behavior within the sliding-surface boundary layer for the case of a constant coefficient in the classical SMC design. In particular, analytical insight is gained on the frequency-scaling behavior of the tracking error under a periodic reference. Simulation and experimental results based on a piezoelectric actuator-based nanopositioner are presented to illustrate the design and analysis, where the hysteresis nonlinearity is represented by a Prandtal–Ishlinskii operator.**

***Index Terms*— Hysteresis, nanopositioning, nonlinear control, piezoelectric actuators, sliding-mode controller (SMC), tracking.**

I. Introduction

HYSTERESIS nonlinearity exists in many control applications, especially in those involving smart material-enabled actuators or sensors. Examples of smart materials are piezoelectrics, magnetostrictives, and shape memory alloys [1]. They are often used in applications that require high accuracy and good resolution, such as nanopositioning. While smart materials have advantages, such as compact size, large bandwidth, and high stiffness [2], they exhibit some nondesirable phenomena, such as hysteresis and creep.

An effective approach to dealing with hysteresis is to use feedforward compensation, where an inverse hysteresis operator is constructed to compensate for the hysteresis effect. This method will reduce the impact of hysteresis appreciably, but due to its open-loop nature, the system performance will depend on the modeling accuracy and the environmental conditions. Consequently, feedback control methods have been proposed in combination with inverse compensation to mitigate the effects of inversion errors and other uncertainties [3]. This general approach to copping with hysteresis is shown in Fig. 1.

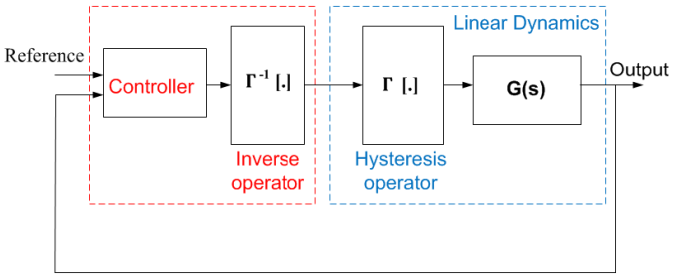

Fig. 1. General control framework for systems preceded by hysteresis.

Hysteresis models can be roughly classified into physical models and phenomenological models. Physical models are based on first principles of physics [4]. Phenomenological models are used to produce behaviors similar to those of the physical systems without necessarily providing physical insight into the problems. A dominant class of phenomenological hysteresis models are formed through weighted superposition of elementary hysteresis units [5], [6], and notable examples of such models include the Preisach operator [7], [8] and the Prandtl–Ishlinskii (PI) operator [6], [9], [10].

Examples of control schemes applied to systems with hysteresis include adaptive control [11], [12], robust control [13]–[23], and adaptive robust control [24]–[26]. Robust control methods span servo-compensator [14], sliding mode controller (SMC) [16]–[20], and H_∞ control [21]–[23]. With these methods, uncertainties in the system are handled without complex adaptation algorithms, and their bounds are typically assumed known. The SMC is attractive because of its robustness against disturbances and parameter uncertainties [27]. Some existing SMC methods for piezo-actuated systems incorporate hysteresis inversion [17], [18], while others do not [16], [19], [20].

In this paper, we advance the study of SMC schemes for systems with hysteresis in several ways. The SMC schemes use a switching function to dominate system uncertainties and force the convergence to the sliding surface. Typically, the coefficient of such a switching function is chosen to be a constant. The choice of this coefficient is generally *ad hoc* and often has to be made through extensive tuning.

Manuscript received September 14, 2013; revised March 10, 2014; accepted May 26, 2014. Date of publication June 20, 2014; date of current version February 11, 2015. Manuscript received in final form May 31, 2014. This work was supported by the National Science Foundation under Grant CMMI 0824830 and Grant CMMI 1301243. Recommended by Associate Editor C. C. Chung.

M. Edardar is with the Department of Electrical and Electronic Engineering, University of Tripoli, Tripoli 13275, Libya (e-mail: moh_edardar@yahoo.com).

X. Tan and H. K. Khalil are with the Department of Electrical and Computer Engineering, Michigan State University, East Lansing, MI 48824 USA (e-mail: xbtan@egr.msu.edu; khalil@egr.msu.edu).

Color versions of one or more of the figures in this paper are available online at http://ieeexplore.ieee.org.

Digital Object Identifier 10.1109/TCST.2014.2329187

The first contribution of this paper lies in the derivation of an analytical bound on the error in approximate hysteresis inversion, which is subsequently exploited to realize a novel design of the switching function that uses a state- and time-dependent coefficient. A general class of hysteresis nonlinearities with piecewise linear characteristics is considered, which encompasses a number of hysteresis operators reported in this paper. The proposed scheme offers a systematic methodology for designing the SMC and eliminates the need for trial-and-error parameter tuning. It also ensures convergence to the sliding surface or a boundary layer of the surface, from any initial conditions of the system and for references with arbitrarily large amplitudes.

The second contribution of this paper is in providing an analytical understanding of the tracking error at the steady state. To make the problem tractable, we limit the analysis to the case with a constant coefficient in the switching function. To avoid control chattering, an SMC is often implemented with the signum function replaced by a saturation function, which acts as a high gain feedback in a boundary layer around the sliding surface. We study the tracking error inside the boundary layer, when the coefficients of the sliding surface are chosen with different orders of magnitude to obtain a multitime-scale structure. This structure is exploited to derive an analytical expression for the tracking error at the steady state under periodic references, and to provide insight into how the error depends on the hysteresis uncertainties, reference frequencies, and controller parameters.

We demonstrate our results using the example of a piezoelectric actuator-based nanopositioner, which exhibits pronounced hysteretic behavior. It is known that using charge control (instead of voltage control) can substantially mitigate the hysteresis effect in piezoelectric actuators [28]. However, drift and saturation problems associated with generally available charge or current amplifiers present hurdles in the adoption of charge control [21]. Despite recent advances made in the design of charge/current amplifiers [29], voltage control remains the popular option for piezoelectric actuators. The nanopositioner is modeled with a PI operator followed by linear dynamics. A PI operator consists of a weighted superstition of play operators, which results in hysteresis loops with piecewise linear segments. Simulation results are presented to support the analysis on the steady-state error for the case with a switching function that has a constant coefficient, as well as to shed insight on the advantages of the proposed scheme with a nonconstant switching coefficient. Experimental results on tracking a number of different references are further provided to demonstrate the effectiveness of the proposed SMC scheme.

Preliminary versions of some results in this paper were presented at the 2012 American Control Conference [30], which dealt with a PI hysteresis model only. Improvements of this paper over [30] include the derivation of inversion error for the wide class of piecewise linear hysteresis models, the analysis of steady-state tracking error in the boundary layer, and the additional experimental results involving new types of reference signals among other things.

The rest of this paper is organized as follows. In Section II, we derive the bounds on the inversion error using the slope and intercept parameters of hysteresis segments, and illustrate the results with the example of a PI operator. This bound is used to design the SMC in Section III, where we establish the tracking performance via Lyapunov analysis. In Section IV, we provide analysis of the tracking error inside the surface boundary layer for the case with constant switching coefficient. Simulation and experimental results are presented in Sections V and VI, respectively. Finally, conclusions are drawn in Section VII.

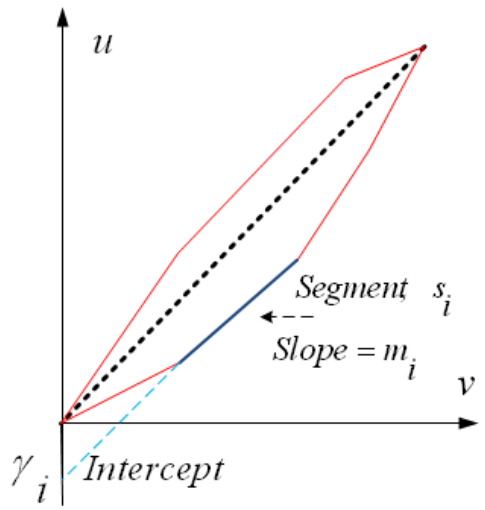

Fig. 2. Illustration of a hysteresis loop with piecewise linear characteristics.

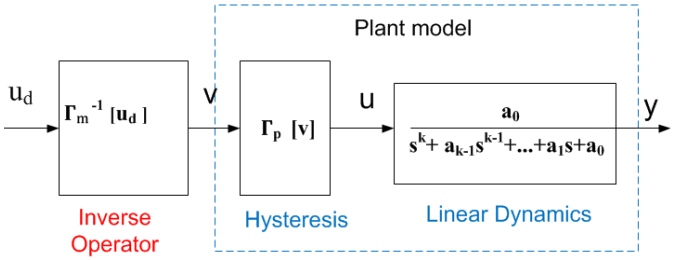

Fig. 3. System with hysteresis preceded by an inverse operator.

II. Characterization of the Inversion Error for Piecewise Linear Hysteresis

In this paper, we consider hysteresis nonlinearities with piecewise linear characteristics, as shown in Fig. 2. Each segment in the hysteresis loop is characterized by its slope m-axis and y-axis intercept γ. Note that a wide class of hysteresis models used in the literature falls under this category, including the piecewise linear model adopted in [3], the PI operator [6], [12], [31], the modified PI operator [10], and the Krasnoselskii–Porkovskii (KP) operator [32] among others. In this section, we first derive the inversion error and its bound for general piecewise linear hysteresis models, and then illustrate the results with a PI operator that has uncertainties in its weight parameters.

A. Inversion Error for Piecewise Linear Hysteresis Characteristics

Fig. 3 shows the system with a feedforward inverse hysteresis compensator, where the plant consists of a hysteresis

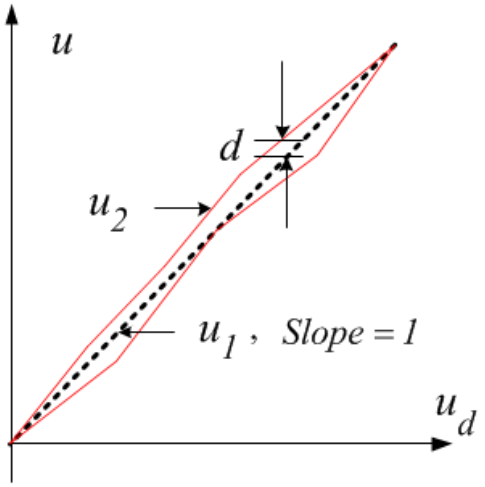

Fig. 4. Illustration of the inversion error.

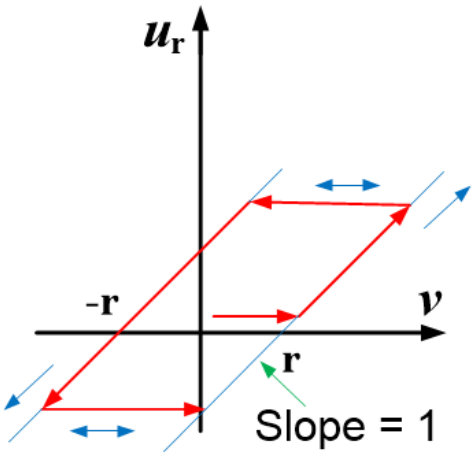

Fig. 5. Play operator.

nonlinearity followed by linear dynamics described by an all-pole transfer function. We assume that the actual hysteresis is represented by an operator Γ_p, and that a nominal model Γ_m for the hysteresis is identified for implementation of Γ_m^{-1}, an approximate inverse to Γ_p. Denote u_d as the control applied to the inverse model and $d = u_d - u$ as the inversion error.

For a given hysteresis segment i with slope m_i and intercept γ_i, the input-output relationship for the hysteresis operator is given by

$$u = m_i v + \gamma_i \tag{1}$$

and for perfect inversion, the input-output relationship for the inverse operator is given by

$$v = \frac{1}{m_i} u_d + \gamma_{\text{inv},i} \tag{2}$$

where $\gamma_{\text{inv},i}$ can be derived as follows. By inserting (2) into (1), we obtain

$$\begin{aligned} u &= m_i \left(\frac{1}{m_i} u_d + \gamma_{\text{inv},i} \right) + \gamma_i \\ &= u_d + m_i \gamma_{\text{inv},i} + \gamma_i \end{aligned} \tag{3}$$

implying

$$\gamma_{\text{inv},i} = -\frac{\gamma_i}{m_i}. \tag{4}$$

To model the uncertainty in hysteresis, we assume that the inverse is still given by (2) and (4) while the actual input-output relationship for segment i is described by

$$u = (m_i + \Delta_{m_i}) v + \gamma_i + \Delta_{\gamma_i} \tag{5}$$

where Δ_{m_i} and Δ_{γ_i} represent the uncertainties in the slope and in the intercept, respectively. Fig. 4 shows how the uncertainties can be used to determine an upper bound on the inversion error. The curve u_1 represents the output u when the inversion is perfect, thus $u_1 = u_d$; u_2 represents the output in the presence of the uncertainties, and by plugging (2) into (5), we obtain

$$u_2(t) = \left(1 + \frac{\Delta_{m_i}}{m_i} \right) u_d(t) + \Delta_{\text{dc},i} \tag{6}$$

where the dc uncertainty $\Delta_{\text{dc},i}$ is defined as

$$\Delta_{\text{dc},i} = \Delta_{\gamma_i} - \frac{\gamma_i \Delta_{m_i}}{m_i}. \tag{7}$$

The difference between u_2 and u_1 represents the uncertainty $d(t)$

$$d(t) = u_2(t) - u_1(t) = \frac{\Delta_{m_i}}{m_i} u_d(t) + \Delta_{\text{dc},i}. \tag{8}$$

The upper bound for d during the hysteresis segment i is then

$$|d(t)| \le \left| \frac{\Delta_{m_i}}{m_i} \right| |u_d(t)| + |\Delta_{\text{dc},i}|. \tag{9}$$

The upper bound for d under all hysteresis segments is

$$|d(t)| \le \left| \frac{\Delta_{m,\max}}{m_{\min}} \right| |u_d(t)| + |\Delta_{\text{dc},\max}| \tag{10}$$

where $m_{\min}$, $|\Delta_{m,\max}|$, and $|\Delta_{\text{dc},\max}|$ are the minimum slope, maximum slope uncertainty, and maximum dc uncertainty, respectively, among all hysteresis segments. In particular, $|\Delta_{\text{dc},\max}|$ is given by

$$|\Delta_{\text{dc},\max}| = |\Delta_{\gamma,\max}| + \frac{|\gamma_{\max}||\Delta_{m,\max}|}{m_{\min}} \tag{11}$$

where $|\gamma_{\max}|$ and $|\Delta_{\gamma,\max}|$ denote the maximum intercept magnitude and maximum intercept uncertainty bound, respectively. It is assumed that $m_{\min} > 0$, which holds true for many hysteresis operators under mild conditions. Equation (10) can be written as

$$|d| \le k_1 |u_d| + k_0 \tag{12}$$

where $k_1 = |\Delta_{m,\max}|/|m_{\min}|$ and $k_0 = |\Delta_{\text{dc},\max}|$.

B. Case Study With the PI Operator

A PI operator consists of a weighted superposition of basic hysteretic units called play operators. While in principle one could consider a continuum of play operators, in practice, the number of play operators is typically chosen to be finite, say $N > 0$. As shown in Fig. 5, a play operator H_r is

characterized by a threshold r, and its output u_r under a continuous, monotone input v can be written as

$$\begin{aligned} u_r(t) &= H_r[v; u_r(0)](t) \\ &= \max(\min(v(t)+r, u_r(0)), v(t)-r) \end{aligned} \tag{13}$$

where $u_r(0)$ denotes the initial condition of the operator. For a general input v, one can break it into monotone segments, and compute the output by setting the final output value under one segment as the initial condition for the next. Note that a play operator can operate in two modes, the linear mode where $u_r(t) = v(t) \pm r$, and the play mode, where $u_r(t)$ remains constant. It is clear that the corresponding slope of the output-input relationship is 1 and 0 under the linear and play modes, respectively. In addition, from Fig. 5

$$|u_r(t)| \leq |v(t)| + r. \tag{14}$$

The output of a PI operator consisting of N play operators is expressed as

$$u(t) = \sum_{j=1}^{N} w_j H_{r_j}[v; u_{r_j}(0)](t) \tag{15}$$

where $\mathbf{w} \stackrel{\triangle}{=} (w_1, w_2, \ldots, w_N)^T$ is the weight vector, and $\mathbf{r} = (r_1, r_2, \ldots, r_N)^T$, with $0 = r_1 < r_2 < \cdots < r_N = r_{\max}$, is the threshold vector. One can easily verify that the hysteresis loops of such a PI operator have piecewise linear characteristics. It is typically assumed that $\mathbf{w} \geq 0$ with $w_1 > 0$, which ensures that $m_{\min}$, the minimum slope of all hysteresis segments, is positive.

For a hysteresis segment i, its slope m_i is given by

$$m_i = \sum_{A_i} w_i \tag{16}$$

where A_i denotes, corresponding to the hysteresis segment i, the set of play operators that are in the linear region. Now, suppose that the actual weight for play operator H_{r_j} is $w_i + \Delta_{w_j}$ with $|\Delta_{w_j}| \leq \Delta_{w,\max} > 0$. From [14], it is straightforward to obtain

$$\Delta_{m_i} = \sum_{j \in A_i} \Delta_{w_j}$$

and thus

$$\Delta_{m,\max} \leq N \Delta_{w,\max}. \tag{17}$$

Finally, using (14), we can derive

$$\gamma_{\max} \leq r_{\max} \sum_{j=1}^{N} w_j \tag{18}$$

$$|\Delta_{\gamma,\max}| \leq N \Delta_{w,\max} r_{\max}. \tag{19}$$

III. Design of the SMC

We consider a plant with linear dynamics of order k, with the transfer function $a_0/s^k + \cdots + a_1 s + a_0$. Note that the linear dynamics are assumed to have a dc gain of 1. This is because any nonunity dc gain can be incorporated into the hysteresis model preceding the dynamics. The linear dynamics can be rewritten as

$$\begin{aligned} \dot{x}_l &= x_{l+1}, \quad 1 \leq l \leq k-1 \\ \dot{x}_k &= -a_{k-1}x_k - a_{k-2}x_{k-1} - \cdots - a_0 x_1 + a_0(u_d + d) \end{aligned} \tag{20}$$

where $y = x_1$ denotes the output, and $a_0 > 0$. The tracking error e_1 is defined as

$$e_1 = y - y_r = x_1 - y_r \tag{21}$$

where y_r is the reference trajectory, which is assumed to have continuous derivatives up to the kth order. To eliminate the dc error at steady state, we add an integrator, the state of which e_0 is defined via $\dot{e_0} = e_1$. Equation (20) can be written in terms of the error as

$$\begin{aligned} \dot{e}_l &= e_{l+1}, \quad 0 \leq l \leq k-1 \\ \dot{e}_k &= -a_{k-1}(e_k + y_r^{(k-1)}) - \cdots - a_0(e_1 + y_r) \\ &\quad + a_0(u_d + d) - y_r^{(k)}. \end{aligned} \tag{22}$$

The sliding surface s is designed in terms of the error

$$s = e_k + \sigma_{k-1}e_{k-1} + \cdots + \sigma_1 e_1 + \sigma_0 e_0. \tag{23}$$

The coefficients $\sigma_0, \sigma_1, \ldots, \sigma_{k-1}$ are chosen such that the polynomial $p^k + \sigma_{k-1}p^{k-1} + \cdots + \sigma_0$ is Hurwitz. To obtain $\dot{s}$, we differentiate both sides of (23), substitute $\dot{e}_k$ from (22), and arrange terms

$$\begin{aligned} \dot{s} = (\sigma_{k-1} - a_{k-1})e_k + \cdots + (\sigma_0 - a_0)e_1 \\ -a_{k-1}y_r^{(k-1)} - \cdots - a_0 y_r + a_0(u_d + d) - y_r^{(k)}. \end{aligned} \tag{24}$$

The control, u_d, is composed of two components, the equivalent component u_{eq} and the switching component u_s

$$u_d = u_{\text{eq}} + u_s. \tag{25}$$

The term u_{eq} eliminates all terms in (24) except for the uncertainty d

$$\begin{aligned} u_{\text{eq}}(t,e) = \frac{1}{a_0}\big[(a_{k-1} - \sigma_{k-1})e_k + \cdots + (a_0 - \sigma_0)e_1 \\ + a_{k-1}y_r^{(k-1)} + \cdots + a_0 y_r + y_r^{(k)}\big] \end{aligned} \tag{26}$$

where $e \stackrel{\triangle}{=} (e_0, e_1, \ldots, e_k)^T$. The uncertainty d is compensated for by the switching component

$$u_s = -\beta \ \text{sgn}(s) \tag{27}$$

where sgn denotes the signum function and β, as described below, is state- and time-dependent. By inserting (25) into (12), we can write the bound on d as

$$\begin{aligned} |d(t)| &\leq k_0 + k_1|u_s(t,e) + u_{\text{eq}}(t,e)| \\ &\leq k_0 + k_1|u_s(t,e)| + k_1|u_{\text{eq}}(t,e)|. \end{aligned} \tag{28}$$

Define

$$\phi(|u_{\text{eq}}(t,e)|) = k_0 + k_1|u_{\text{eq}}(t,e)| \tag{29}$$

which implies

$$|d(t)| \leq \phi(|u_{\text{eq}}(t,e)|) + k_1|u_s(t,e)|. \tag{30}$$

Substituting (25) and (26) in (24), we obtain

$$\dot{s} = a_0(d(t) + u_s(t,e)). \tag{31}$$

For the stability analysis, we define a Lyapunov function $V = 1/2s^2$. Then, by taking the derivative of V, we can show that, if $k_1 < 1$, then $\dot{V} < -a_0 b_0 |s|$ for

$$\beta(t,e) = \frac{\phi(|u_{\text{eq}}(t,e)|)}{1-k_1} + b_0 \tag{32}$$

where b_0 is a small positive number. In practical implementation, a strict signum function as in (27) could cause chattering around $s = 0$. To avoid this problem, we will use the following form of switching function, where the saturation function $\text{sat}(\cdot)$ replaces $\text{sgn}(\cdot)$ [33]

$$u_s = -\beta(t,e)\text{sat}\left(\frac{s}{\mu}\right) \tag{33}$$

and the parameter $\mu > 0$ determines the size of the boundary layer for the sliding surface s. Note that $\text{sat}(s/\mu)$ is equal to $\text{sgn}(s)$ for $|s| > \mu$ and equal to s/μ otherwise. With (33), it can be shown that the tracking error converges to an ultimate bound, which is determined by the choice of μ.

The proposed design of a state- and time-dependent switching function eliminates the need for parameter tuning as typically required in a traditional SMC design approach, where a constant β is adopted in the switching control. The second major contribution of this paper is to provide new analytical results on the tracking error when an SMC with constant β is used, as detailed in Section IV. That design requires us to limit the system variables to a compact set $\Omega = \{\eta^T P \eta \le c_1\} \times \{|s| \le c_2\}$, where $\eta = [e_0\ e_1\ \dots\ e_{k-1}]$, $\dot{\eta} = A\eta + Bs$. The matrix A and the vector B are in the controller canonical form with the last row $[-\sigma_0\ -\sigma_1 \cdots -\sigma_{k-1}]$ in A. The matrix P is the solution of the Lyapunov equation $PA + A^T P = -I$ and c_1 and c_2 are constants. For more details, refer to [33]. It is noted that the bound obtained for a constant β is very conservative and large because it needs to accommodate all operating frequencies and reference trajectories among other factors. In practice, one typically has to tune the value of constant β through extensive simulation and experimentation.

A. System Scaling

When the linear system has a large bandwidth, as that for the nanopositioner to be used later in the simulation and experiments, the coefficients $(\sigma_0, \dots, \sigma_{k-1})$ for the sliding surface and the parameter μ for the boundary layer thickness will also be relatively large, in proper orders of the bandwidth of the dynamics.

We show this through a scaling argument for a second-order system, which can be readily generalized for higher order ones. With ω_n as the natural frequency of the system, we have $a_0 = \omega_n^2$ and $a_1 = 2\zeta\omega_n$, where ζ is the damping coefficient. The augmented integral control $\dot{e}_0 = e_1$. The closed-loop system is given by

$$\begin{aligned}
\dot{e}_0 &= e_1 \\
\dot{e}_1 &= e_2 \\
\dot{e}_2 &= -a_1(e_2 + \dot{y}_r) - a_0(e_1 + y_r) + a_0(u_d + d) - \ddot{y}_r.
\end{aligned} \tag{34}$$

For scaling the system, we apply the change of variables $\tau = \omega_n t$, $z_0 = e_0\omega_n$, $z_1 = e_1$, and $z_2 = e_2/\omega_n$. This will result in a transformed system

$$\begin{aligned}
\frac{dz_0}{d\tau} &= z_1 \\
\frac{dz_1}{d\tau} &= z_2 \\
\frac{dz_2}{d\tau} &= -2\zeta z_2 - z_1 + u_d + d - \frac{1}{\omega_n^2}\left(\ddot{y}_r + 2\zeta\omega_n\dot{y}_r + \omega_n^2 y_r\right).
\end{aligned} \tag{35}$$

Now for the transformed system, with the surface chosen as $s = z_2 + \breve{\sigma}_1 z_1 + \breve{\sigma}_0 z_0$ and for a boundary layer constant $\breve{\mu}$, the switching component of the control is

$$u_s = -\beta\ \text{sat}\left(\frac{s}{\breve{\mu}}\right) = -\beta\ \text{sat}\left(\frac{z_2 + \breve{\sigma}_1 z_1 + \breve{\sigma}_0 z_0}{\breve{\mu}}\right). \tag{36}$$

Then, we substitute the original coordinates into (36) to obtain

$$\begin{aligned}
u_s &= -\beta\ \text{sat}\left(\frac{e_2 + \breve{\sigma}_1\omega_n e_1 + \breve{\sigma}_0\omega_n^2 e_0}{\breve{\mu}\omega_n}\right) \\
&= -\beta\ \text{sat}\left(\frac{e_2 + \sigma_1 e_1 + \sigma_0 e_0}{\mu}\right).
\end{aligned} \tag{37}$$

From (37), we can see that the parameters of the sliding surface for the nonscaled system related to those of the scaled one as $\sigma_0 = \breve{\sigma}_0\omega_n^2$, $\sigma_1 = \breve{\sigma}_1\omega_n$, and $\mu = \breve{\mu}\omega_n$.

IV. Analysis of the Tracking Error Inside the Boundary Layer

In this section, we investigate the tracking error inside the boundary layer of the switching surface when β is constant. The purpose is to derive an analytical expression for the error and its bound and shed light on how the error depends on the modeling error and other system parameters.

A. Singular Perturbation Analysis

The saturation function becomes linear inside the boundary layer, $|s| < \mu$, with $\beta\ \text{sat}(s/\mu) = \beta s/\mu$. To find an expression for $\dot{e} = [\dot{e}_0\ \dot{e}_1 \dots \dot{e}_k]^T$, we insert d from (8) into $\dot{e}_k$ of (22), substitute both u_{eq} and $u_s = -\beta s/\mu$ into $\dot{e}_k$, and simplify terms. Note that the forthcoming differential equations are given for any segment in the hysteresis-loop

$$\begin{aligned}
\dot{e}_k = &\left[\left(1 + \frac{\Delta_{m_i}}{m_i}\right)\left(\frac{-a_0\beta}{\mu} - \sigma_{k-1}\right) + a_{k-1}\frac{\Delta_{m_i}}{m_i}\right]e_k \\
&+ \left[\left(1 + \frac{\Delta_{m_i}}{m_i}\right)\left(\frac{-a_0\beta\sigma_{k-1}}{\mu} - \sigma_{k-2}\right) + a_{k-2}\frac{\Delta_{m_i}}{m_i}\right]e_{k-1} \\
&+ \cdots + \left[\left(1 + \frac{\Delta_{m_i}}{m_i}\right)\left(\frac{-a_0\beta\sigma_1}{\mu} - \sigma_0\right) + a_0\frac{\Delta_{m_i}}{m_i}\right]e_1 \\
&+ \left[\left(1 + \frac{\Delta_{m_i}}{m_i}\right)\left(\frac{-a_0\beta}{\mu}\sigma_0\right)\right]e_0 + a_0\Delta_{\text{dc},i} + \frac{\Delta_{m_i}}{m_i}y_r^{(k)} \\
&+ a_{k-1}\frac{\Delta_{m_i}}{m_i}y_r^{(k-1)} + \cdots + a_1\frac{\Delta_{m_i}}{m_i}\dot{y}_r + a_0\frac{\Delta_{m_i}}{m_i}y_r.
\end{aligned} \tag{38}$$

We divide both sides of (38) by $a_0\beta/\mu$. For $l = 1, \ldots, k$, define

$$\delta_l \triangleq \frac{\mu}{a_0\beta}\left(\sigma_{l-1} - a_{l-1}\frac{\Delta_{m_i}}{m_i}\right).$$

Equation (38) can then be written in the form

$$\varepsilon_k \dot{e_k} = \left(1+\frac{\Delta_{m_i}}{m_i}\right)\left[-(1+\delta_k)e_k - (\sigma_{k-1}+\delta_{k-1})e_{k-1} - \cdots - (\sigma_1+\delta_1)e_1 - \sigma_0 e_0\right] + \frac{\mu}{\beta}\Delta_{\mathrm{dc},i} + \frac{\Delta_{m_i}}{m_i}\frac{\mu}{\beta}\left(\frac{y_r^{(k)}}{a_0} + \frac{a_{k-1}}{a_0}y_r^{(k-1)} + \cdots + \frac{a_1}{a_0}\dot{y}_r + y_r\right) \tag{39}$$

where $\varepsilon_k = \mu/a_0\beta$. Define $\lambda = \sigma_0/\sigma_1 + \delta_1$. In order to solve the differential equations of the system, we make the following assumptions.

1) For the system to be represented in a singularly perturbed multitime-scale structure, we require that $\varepsilon_k \ll \varepsilon_{k-1} = 1 + \delta_k/\sigma_{k-1} + \delta_{k-1} \ll \cdots \ll \varepsilon_l = \sigma_{l+1} + \delta_{l+1}/\sigma_l + \delta_l \ll \cdots \ll \varepsilon_1 = \sigma_2 + \delta_2/\sigma_1 + \delta_1 \ll 1/\lambda \ll 1$. This is the second assumption about σ_i's. The first was about the construction of the sliding surface, where these coefficient are chosen to make a polynomial Hurwitz. It is not difficult to satisfy both conditions. For instance, taking

$$\sigma_{k-1} = \alpha^k,\ \frac{\sigma_{k-2}}{\sigma_{k-1}} = \alpha^{k-1},\ \ldots,\ \frac{\sigma_2}{\sigma_1} = \alpha^2, \frac{\sigma_0}{\sigma_1} = \alpha \tag{40}$$

it can be seen that for sufficiently large $\alpha > 0$, the polynomial $p^k + \sigma_{k-1}p^{k-1} + \cdots + \sigma_1 p + \sigma_0$ can be factored as $(p + n_k\alpha^k)(p + n_{k-1}\alpha^{k-1})\cdots(p + n_1\alpha)$, where n_1 to n_k can be made arbitrarily close to one. Hence, the roots of the polynomial can be made arbitrarily close to $-\alpha,\ -\alpha^2 \cdots - \alpha^k$. With α fixed, the condition (40) can be satisfied by choosing μ small enough.

2) The magnitude of the slope uncertainty in each segment i is smaller than the slope itself, $|\Delta_{m_i}| < |m_i|$. This assumption implies $\mathrm{sgn}(m_i) = \mathrm{sgn}(m_i + \Delta_{m_i})$. By nested application of the singular perturbation method [34], we obtain an analytical approximation to the tracking error e_1. This process is shown below by an example of a second-order system.

1) Example: Let $k = 2$, $\varepsilon_1 = 1 + \delta_2/\sigma_1 + \delta_1$, and $\varepsilon_2 = \mu/a_0\beta$. By using (38), the second-order closed-loop system is given by

$$\begin{aligned}
\dot{e_0} &= e_1\\
\dot{e_1} &= e_2\\
\dot{e_2} &= \frac{a_0\beta}{\mu}\left[\left(1+\frac{\Delta_{m_i}}{m_i}\right)[-(1+\delta_2)e_2 - (\sigma_1+\delta_1)e_1 - \sigma_0 e_0] + \frac{\mu}{\beta}\Delta_{\mathrm{dc},i} + \frac{\Delta_{m_i}}{m_i}\frac{\mu}{\beta}\left(\frac{\ddot{y}_r}{a_0} + \frac{a_1}{a_0}\dot{y}_r + y_r\right)\right].
\end{aligned} \tag{41}$$

To present the system in a multitime-scale form, let us define $\bar{e}_2 = \varepsilon_1 e_2$. The system is represented in the singularly perturbation form as

$$\begin{aligned}
\dot{e_0} &= e_1\\
\varepsilon_1\dot{e_1} &= \bar{e}_2\\
\varepsilon_2\dot{\bar{e}}_2 &= \left(1+\frac{\Delta_{m_i}}{m_i}\right)\left[-(1+\delta_2)\bar{e}_2 - (1+\delta_2)e_1 - \sigma_0\frac{1+\delta_2}{\sigma_1+\delta_1}e_0\right] + \frac{1+\delta_2}{\sigma_1+\delta_1}\left[\frac{\mu}{\beta}\Delta_{\mathrm{dc},i} + \frac{\Delta_{m_i}}{m_i}\frac{\mu}{\beta}\left(\frac{\ddot{y}_r}{a_0} + \frac{a_1}{a_0}\dot{y}_r + y_r\right)\right].
\end{aligned} \tag{42}$$

By having $\varepsilon_2 \ll \varepsilon_1 \ll 1$, we guarantee that the system of (42) has a multitime-scale structure.

Setting $\varepsilon_2 = 0$, we can express $\bar{e}_2$, we can express $\dot{e}_1$ equation. The reduced system can be presented as a singularly perturbed system again

$$\begin{aligned}
\dot{e_0} &= e_1\\
\varepsilon_1\dot{e_1} &= -e_1 - \frac{\sigma_0}{\sigma_1+\delta_1}e_0 + \frac{\mu}{(\sigma_1+\delta_1)\beta}\frac{m_i\Delta_{\mathrm{dc},i}}{m_i+\Delta_{m_i}} + \frac{\mu}{(\sigma_1+\delta_1)\beta}\frac{\Delta_{m_i}}{m_i+\Delta_{m_i}}\left(\frac{\ddot{y}_r}{a_0} + \frac{a_1}{a_0}\dot{y}_r + y_r\right).
\end{aligned} \tag{43}$$

By setting $\varepsilon_1 = 0$, we obtain

$$e_1 = -\frac{\sigma_0}{(\sigma_1+\delta_1)}e_0 + \frac{\mu}{(\sigma_1+\delta_1)\beta}\frac{m_i\Delta_{\mathrm{dc},i}}{m_i+\Delta_{m_i}} + \frac{\mu}{(\sigma_1+\delta_1)\beta}\frac{\Delta_{m_i}}{m_i+\Delta_{m_i}}\left(\frac{\ddot{y}_r}{a_0} + \frac{a_1}{a_0}\dot{y}_r + y_r\right). \tag{44}$$

Since $\dot{e_0} = e_1$, at this point we arrive at a scalar differential equation in one variable e_0, which can be solved to get e_0 and then subsequently e_1 with (44). We can follow the procedure in this example for a kth order system. In that case, the tracking error $e_1 = \dot{e}_0$ is given by

$$\dot{e}_0 = -\frac{\sigma_0}{\sigma_1+\delta_1}e_0 + \frac{\mu}{(\sigma_1+\delta_1)\beta}\frac{m_i\Delta_{\mathrm{dc},i}}{m_i+\Delta_{m_i}} + \frac{\mu}{(\sigma_1+\delta_1)\beta} \times \frac{\Delta_{m_i}}{m_i+\Delta_{m_i}}\left(\frac{y_r^{(k)}}{a_0} + \frac{a_{k-1}}{a_0}y_r^{(k-1)} + \cdots + \frac{a_1}{a_0}\dot{y}_r + y_r\right). \tag{45}$$

Note that the solution of (45) only depends on σ_0 and σ_1 while the other parameters of the surface (σ_2 or higher) are part of the fast transient of the original system, which is approximated using the singular perturbation method. The above steps show how we obtain e_0 for a given hysteresis segment i. In order to accommodate the effect of traversing from one segment to another, we follow the procedure described below, where we consider a sinusoidal reference for ease of presentation.

B. Tracking Error for a Sinusoidal Reference

In order to discuss how the error scales with frequency, a sinusoidal reference $y_r = A_c\sin(\omega t)$ is applied to the system. We assume that the solution of the closed-loop system converges to a periodic function with the same period T of the reference input. This assumption is reasonable in view of

the simulation and experimental results in this paper and also in [14], [15], [17], [35], and [18].

The idea of getting a solution that shows the impact of all hysteresis segments on each other is explained by the following steps, which are analogous to those for analyzing a proportional-integral (PI) controlled system in [36]. We start by solving (45) for the segment i with initial value $e_0(t_i)$, where $i = 1, \ldots, L$ and L is the number of segments of a hysteresis-loop at the steady state. Then, the final value of this segment $e_0(t_{i+1})$ will serve as the initial value for the following segment $i+1$. We continue this process around one cycle until we get $e_0(t_i + T)$. The periodicity of the solution implies that $e_0(t_i + T) = e_0(t_i)$, which allows us to obtain an expression for $e_0(t_i)$. By substituting this expression in the solution of (45), we get $e_0(t)$, $t_i \leq t < t_{i+1}$, and then segment by segment, we can get $e_0(t)$ for the rest of the cycle. Subsequently, the tracking error e_1 is obtained via $e_1 = \dot{e}_0$.

With $y_r = A_c \sin\omega t$ and (45), one obtains

$$\dot{e}_0 = -\lambda e_0 + \mathcal{K}_i + \mathcal{M}_i \sin\omega t + \mathcal{N}_i \cos\omega t. \tag{46}$$

Here, without loss of generality, we can take the dimension of the linear dynamics k as an even number, which is common in linear systems with complex modes. From (45), we have

$$\mathcal{K}_i = \frac{\mu}{(\sigma_1+\delta_1)\beta}\frac{m_i\Delta_{\mathrm{dc},i}}{m_i+\Delta_{m_i}}$$

$$\mathcal{M}_i = \frac{\mu A_c}{(\sigma_1+\delta_1)\beta}\frac{\Delta_{m_i}}{m_i+\Delta_{m_i}}\left(1-\frac{a_2}{a_0}\omega^2+\cdots+(-1)^{k/2}\frac{\omega^k}{a_0}\right)$$

and

$$\mathcal{N}_i = \frac{\mu A_c}{(\sigma_1+\delta_1)\beta}\frac{\Delta_{m_i}}{m_i+\Delta_{m_i}} \times\left(\frac{a_1}{a_0}\omega-\frac{a_3}{a_0}\omega^3+\cdots+(-1)^{(k-2)/2}\frac{a_{k-1}}{a_0}\omega^{k-1}\right).$$

Note that if k is an odd number, we only need to redefine the quantities $\mathcal{M}_i$ and $\mathcal{N}_i$. The solution of the first-order equation (46) is

$$\begin{aligned} e_0(t) = {} & e^{-\lambda(t-t_i)}e_0(t_i) + \frac{\mathcal{K}_i}{\lambda}\left[1-e^{-\lambda(t-t_i)}\right] \\ & + \frac{\mathcal{M}_i}{\lambda^2+\omega^2}\left[(\lambda\sin\omega t-\omega\cos\omega t) - e^{\lambda(t-t_i)}\right. \\ & \qquad \left.(\lambda\sin\omega t_i-\omega\cos\omega t_i)\right] \\ & + \frac{\mathcal{N}_i}{\lambda^2+\omega^2}\left[(\lambda\cos\omega t+\omega\sin\omega t)e^{-\lambda(t-t_i)}\right. \\ & \qquad \left.(\lambda\cos\omega t_i+\omega\sin\omega t_i)\right]. \end{aligned} \tag{47}$$

From (46), it can be shown that the tracking error e_1 at the steady state is composed of periodic, exponentially decaying terms and sinusoidal terms. The decaying terms can be made decrease fast by making λ large enough. Let us investigate closely the effect of different parameters on the nondecaying sinusoidal terms. It can be shown that at the steady state

$$\begin{aligned} e_1(t) = {} & \varrho_i(\lambda\sin\omega t-\omega\cos\omega t) + \mathcal{M}_i\sin\omega t \\ & + \varpi_i(\lambda\cos\omega t+\omega\sin\omega t) + \mathcal{N}_i\cos\omega t \end{aligned} \tag{48}$$

where $\varrho_i = -\lambda\mathcal{M}_i/\lambda^2+\omega^2$, and $\varpi_i = -\lambda\mathcal{N}_i/\lambda^2+\omega^2$. To see how we can use (48) to calculate the bound on the tracking error, let us go back to our example with the second-order linear dynamics and substitute $\varrho_i, \varpi_i, \mathcal{M}_i, \mathcal{N}_i$ by their equivalent expressions in (48). We also approximate $(\sigma_1+\delta_1)$ by σ_1

$$e_1(t) = \frac{\mu A_c}{\sigma_1\beta}\frac{\Delta_{m_i}}{m_i}[A_1(\omega)\sin\omega t + A_2(\omega)\cos\omega t] \tag{49}$$

where

$$A_1(\omega) = \left(\frac{\omega^2}{\lambda^2+\omega^2}\left[1-\frac{\omega^2}{a_0}\right]-\frac{\lambda\omega}{\lambda^2+\omega^2}\left[\frac{a_0}{a_1}\omega\right]\right)$$

and

$$A_2(\omega) = \left(\frac{\omega^2}{\lambda^2+\omega^2}\left[\frac{a_0}{a_1}\omega\right]+\frac{\lambda\omega}{\lambda^2+\omega^2}\left[1-\frac{\omega^2}{a_0}\right]\right).$$

The error size depends on how the frequency ω is related to the parameter $\lambda = \sigma_0/\sigma_1$.

We see from (49) that the sinusoidal portion of the error is proportional to the segment slope uncertainty Δ_{m_i}, the size of the reference input A_c, and the chosen size of the boundary layer μ. However, we can reduce this error by increasing σ_1 or β. We know that β is the amplitude of the switching component of the control signal, which is constrained by the actuator limits. By increasing σ_1, we are also required to increases σ_0 and this leads to using high gains.

For frequencies $\omega \ll \lambda$, the error $e_1(t) \propto \omega/\lambda$ and increases as the frequency increases. However, when $\lambda \ll \omega \ll \omega_n = \sqrt{a_0}$, the error will be in the form $e_1(t) \cong \mu A_c/\sigma_1\beta\Delta_{m_i}/m_i(\sin\omega t + \lambda/\omega\cos\omega t)$. The cosine term decreases as we increase the frequency, which causes the error to decrease. At higher frequencies that approach the resonance frequency, the terms dependent on $a_0 = \omega_n^2$ and $a_1 = 2\zeta\omega_n$ start to be effective and contribute to the total error.

The upper bound on e_1 can be obtained from (49) as

$$|e_1(t)| \leq \frac{\mu A_c}{\sigma_1\beta}\frac{|\Delta_{m,\max}|}{m_{\min}}\sqrt{A_1^2(\omega)+A_2^2(\omega)}. \tag{50}$$

V. Simulation Results

Control of a commercial nanopositioner (Nano-OP65 with Nano Drive controller, Mad City Labs Inc.) is used to demonstrate the results. The simulation is based on the experimentally identified model of the nanopositioner. The piezo-actuated positioner has a total travel range of 65 μm, and has a built-in capacitive sensor that measures its displacement output. The Nano Drive controller contains low-noise, low-drift power amplifier for driving the piezoelectric actuator, and has other functions such as realizing PI closed-loop control. In this paper, the Nano Drive controller is solely used as a power amplifier; data acquisition and control are realized through a dSPACE system (RT1104, dSPACE). A picture of the nanopositioner, its power amplifier (Nano Drive), and the data acquisition interface is shown in Fig. 6.

The linear dynamics are fitted experimentally with a second-order system with the transfer function $a_0/s^2+a_1s+a_0$, where $a_1 = 5.743 \times 10^3$ and $a_0 = 1.717 \times 10^8$, implying a resonant frequency of $\omega_n = 1.3 \times 10^4$ rad/s. The hysteresis is modeled with a PI-operator with five play operators with thresholds $\mathbf{r} = [0,\ 0.63,\ 1.27,\ 2.54,\ 4.45]^T$ and the

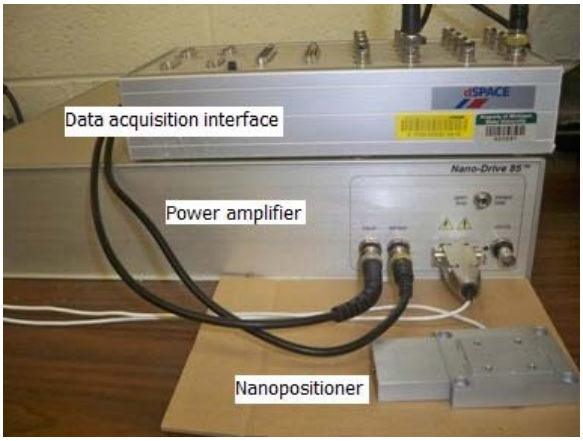

Fig. 6. Experimental setup including the nanopositioner, power amplifier, and data acquisition interface.

vector of weights for the operator is $\mathbf{w} = [5.88,\ 1.58,\ 0.47,\ 0.98,\ 0.4]^T$. For the purpose of simulation, we perturb each component of the weight vector by $\Delta_{w,\max} = 0.15$. This perturbation is chosen such that the obtained inversion error has a size close to what we have observed in experiments when the inverse operator is cascaded with the real nanopositioner. We calculate the corresponding maximum uncertainties on the slopes as $|\Delta_{\mathrm{m},\max}| = 0.75$ and $|\Delta_{\gamma,\max}| = 3.3$. The calculated constants for the inversion error bound (12) of the switching control are $k_1 = 0.13$ and $k_0 = 8.6$. The inversion of the PI operator is realized through another PI operator, the thresholds and weights of which are computed as described in [10].

The simulation results consist of mainly two parts. In the first part, we show the advantage of the proposed SMC scheme with state- and time-dependent β. Fig. 7 shows that, for a sinusoidal reference with a range of 70 μm, both the proposed SMC scheme and an SMC scheme with a constant $\beta = 10$ are able to achieving good tracking. However, as shown in Fig. 8, when the range of the reference is increased to 130 μm, the scheme with the constant β is no longer able to dominate the impact of the hysteresis inversion error and results in instability. In contrast, the proposed scheme tracks the new reference well without the need for parameter retuning.

In the second part of the simulation results, we validate the tracking error analysis presented in Section IV, when a constant β is used. As commented in Section III, rigorous choice of such a β would result in very conservative, impractical values for β. Hence, a trial-and-error approach is used here to pick the values for β. Note that our focus is on the validation of the analytical approximation for the inversion error and exploration of the factors affecting the error. In Fig. 9, we compare the maximum amplitudes of the tracking error obtained through simulation and through analysis (50), respectively, when the reference signal is a sinusoid with amplitude of 25 μm and frequency ranging from 1 to 3000 Hz. In this plot $\beta = 12.5$ is used. The sliding surface coefficients are chosen as $\sigma_1 = 3\times10^4$ and $\sigma_0 = 3\times10^6$ while the boundary layer parameter is $\mu = 2\times10^4$. The value of μ is chosen in the order of σ_1. These values are chosen high

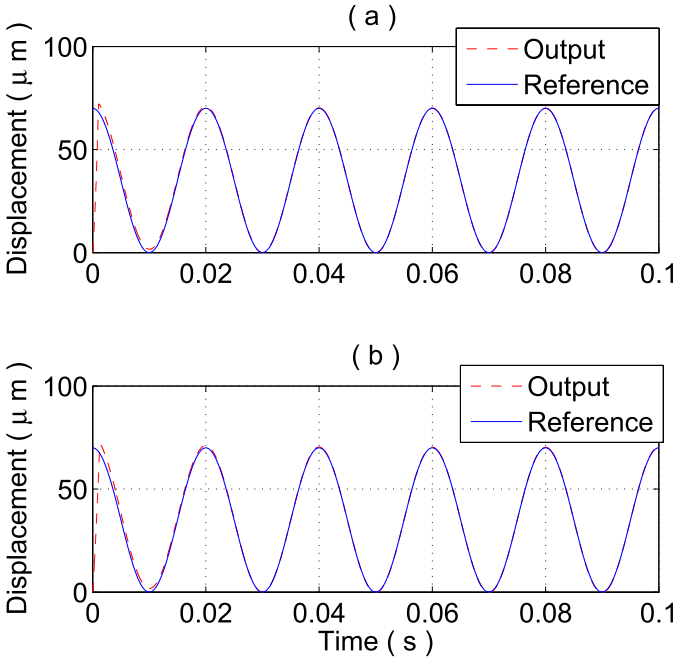

Fig. 7. Tracking performance for a reference with range of 70 μm. (a) State- and time-dependent β. (b) Constant $\beta = 10$.

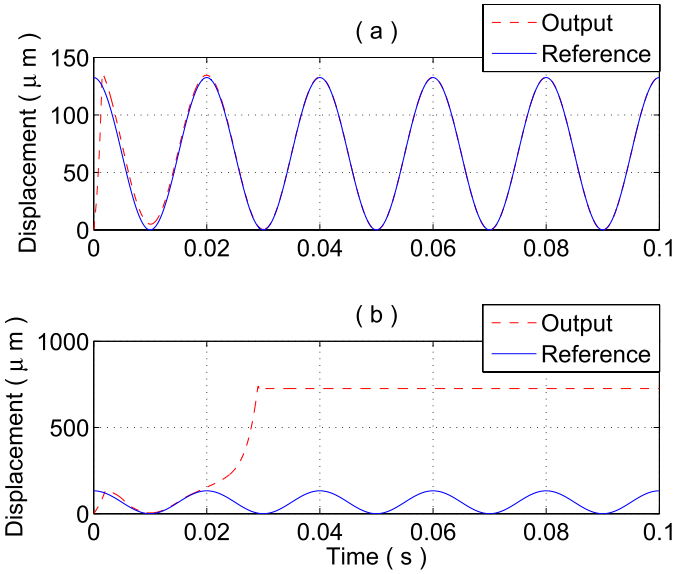

Fig. 8. Tracking performance for a reference with range of 130 μm. (a) State- and time-dependent β. (b) Constant $\beta = 10$.

because the actuator has large bandwidth ω_n. The normalized values can be calculated as explained in the system scaling part toward the end of Section III.

From Fig. 9, we notice the following. The error obtained in simulation increases with the frequency up to 50 Hz, then it remains almost constant for the midfrequency range until about 400 Hz, and then it starts to decrease before it increases again at higher frequencies. The analytical error bound shows similar characteristics for all frequencies, thus supporting the validity of the presented analysis.

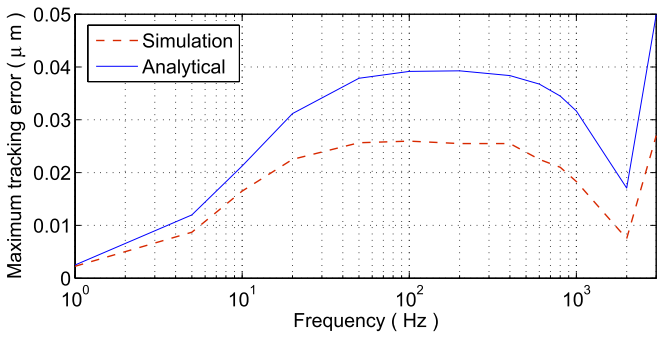

Fig. 9. Comparison of simulation and analytical results on the tracking error at different frequencies.

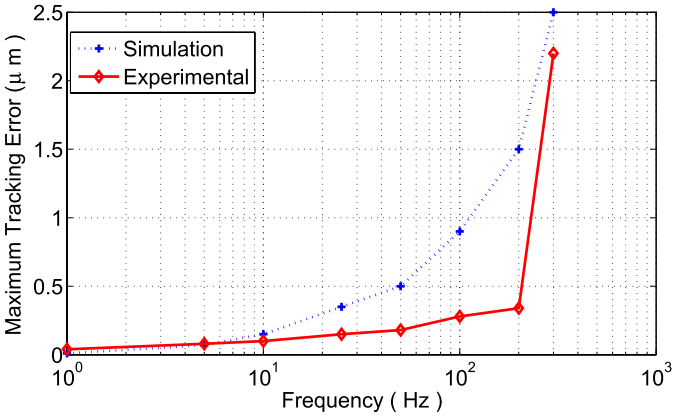

Fig. 10. Comparison of maximum tracking errors observed in experimental and simulation results, when the rate limiter is included in the simulated system.

TABLE I
EXPERIMENTAL COMPARISON BETWEEN MAXIMUM TRACKING ERRORS (μm) FOR SMC AND PI CONTROL

frequencies	SMC–controller	PI–controller
	Max $\lvert e(t)\rvert$	Max $\lvert e(t)\rvert$
1 Hz	0.05	0.025
10 Hz	0.08	0.2
20 Hz	0.12	0.38
50 Hz	0.14	0.8
100 Hz	0.24	1.4
200 Hz	0.35	3.0

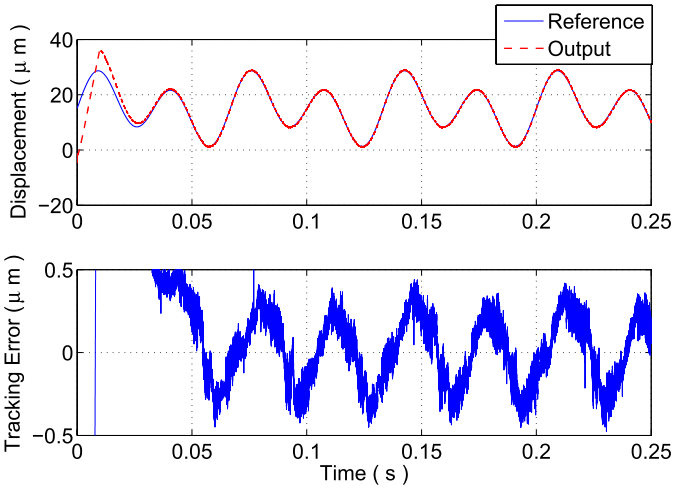

Fig. 11. Experimental results on tracking a multifrequency reference using the proposed SMC scheme.

VI. EXPERIMENTAL RESULTS

In this section, we present experimental results on tracking various reference signals using the proposed SMC method with a state- and time-dependent β. Since the velocity of the nanopositioner is not available for measurement, a linear observer is used to estimate the velocity for the closed-loop system. During the experiments, an important safety mechanism is a rate limiter implemented in dSPACE, to protect the positioner from sudden changes of the applied voltage. The rate limiter modifies the control input to meet the rate constraint, but also distorts the control signal when tracking relatively high-frequency references. Specifically, it introduces a phase lag between the reference signal and the output, causing a larger tracking error. To show this, a rate limiter is added to the simulated system, and as shown in Fig. 10, the rise of the maximum tracking error with frequency for the simulated system shares a similar trend with that for the experimental system. Here, the reference trajectories are sinusoidal signals with amplitudes of 20 μm and frequencies ranging from 1 to 300 Hz.

In Table I, we further compare the proposed SMC scheme and a PI controller on the maximum tracking error under the aforementioned sinusoidal references. The results of the PI control are obtained from [37]. It is obvious form Table I that the proposed controller outperforms the conventional PI controller at all frequencies, except at a very low frequency (1 Hz), where they have comparable performance. We note that, while the PI controller is popular and adequate for many industrial applications requiring low-bandwidth operations, in general, a controller that enables higher bandwidth (before the onset of excited vibrations) is of interest. Even in the domain of nanopositioning, there are applications (for example, fast-speed atomic force microscopy) where higher speeds of operation would be welcome. Therefore, it is instrumental to compare the controllers at frequencies beyond a few Hz, the typical bandwidth range for commercial PI controllers.

Additional nonsinusoidal reference signals are also applied to examine the performance of the proposed controller. Fig. 11 shows the results on tracking a multifrequency reference composed of two sinusoidal signals of frequencies 15 and 30 Hz, while in Fig. 12 shows the tracking results under a reference that generated using a van der Pol oscillator. In both Figs. 11 and 12, the proposed controller succeeds in tracking the reference trajectories with small tracking errors of $<$0.5 μm. A further comparison of tracking errors under the multisine frequency reference for the SMC scheme and the PI controller is shown in Fig. 13. This figure not only confirms the observation from Table I that the proposed SMC scheme outperforms the PI controller as the steady state, but

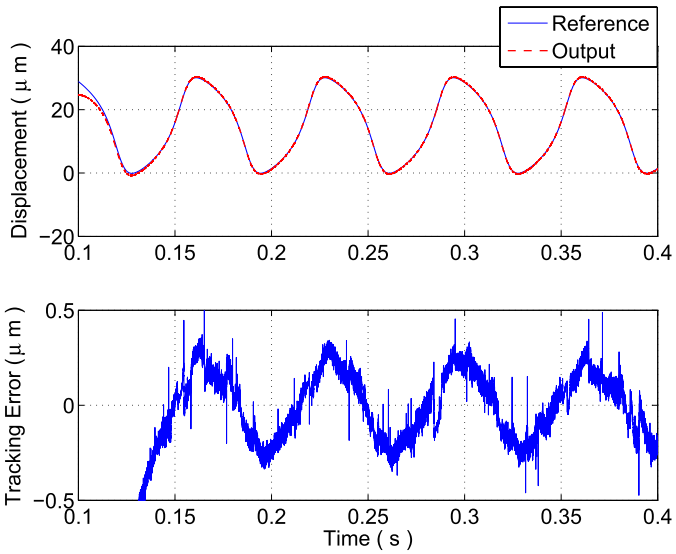

Fig. 12. Experimental results on tracking a van der Pol oscillator-generated reference using the proposed SMC scheme.

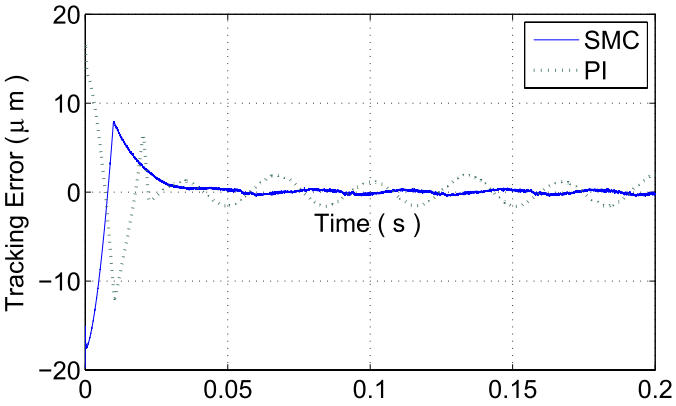

Fig. 13. Comparison of experimental tracking errors under the multisine reference.

also demonstrates the advantages of the SMC scheme during the transients. In particular, the latter scheme shows faster transients and smaller oscillations than the PI controller.

Finally, we note that, from Figs. 11 and 12, the SMC scheme results in apparent high-frequency oscillations in the tracking error. Since the corresponding reference signals have frequency components lower than 50 Hz, those oscillations are not believed to be caused by the excited vibration of the nanopositioner, which has a resonant frequency of over 2000 Hz. Instead, the cause of the observed oscillations is likely the chattering of the SMC, due to the relatively small μ (close to 1 after the aforementioned scaling) for the saturation function, unmodeled system dynamics and nonlinearities, delay in the digital control system, and other nonideal factors in the experiments.

VII. Conclusion

Hysteresis nonlinearity is a main challenge in many applications that require tracking control. A general approach to dealing with this issue is to use hysteresis-inverse compensation integrated with feedback control. In this paper, we derived a bound on the inversion error using the slope-intercept parameters of piecewise linear hysteresis loops. This bound was used in the design of an SMC with a state- and time-dependent switching function β. The approach ensures the convergence to the boundary layer of the sliding surface without imposing a compactness assumption, and eliminates the need for parameter tuning as required for the design of a constant β in the classical approach. Furthermore, using multitime-scale analysis, we derived an expression for the tracking error inside the boundary layer of the sliding surface for the case of a constant switching function β. It was shown that the error is proportional to the chosen boundary layer size (μ) and inversely proportional to the coefficient of the error term (σ_1) in the surface equation as well as the amplitude of the saturation function (β) of the control signal. In particular, the expression of the tracking error shows how the error scales with frequency. It was shown analytically and by simulation that the error increases in the first portion ($\omega < \lambda$) of range of interest and stays constant before it is affected by resonance frequencies and fast dynamics. Experiments were conducted for a pizeo-electric actuator, where the results confirmed the effectiveness of the proposed SMC design in the tracking of a number of different reference signals.

Our design and analysis was limited to the case where the linear plant had no zeros. In future work, we plan to extend the proposed approach to systems with zero dynamics, including the case with unstable zero dynamics. We will also explore the application of the approach to other piecewise linear hysteresis models, such as the modified PI operator and the KP operator.

References

[1] R. Smith, *Smart Material Systems: Model Developments*. Philadelphia, PA, USA: SIAM, 2005.
[2] S. Devasia, E. Eleftheriou, and S. O. Moheimani, "A survey of control issues in nanopositioning," *IEEE Trans. Control Syst. Technol.*, vol. 15, no. 5, pp. 802–823, Sep. 2007.
[3] G. Tao and P. Kokotovic, "Adaptive control of plants with unknown hystereses," *IEEE Trans. Autom. Control*, vol. 40, no. 2, pp. 200–212, Feb. 1995.
[4] D. Jiles and D. Atherton, "Theory of ferromagnetic hysteresis," *J. Magn. Magn. Mater.*, vol. 61, nos. 1–2, pp. 48–60, 1986.
[5] M. Krasnoselskii and A. Pokrovskii, *Systems With Hysteresis*. New York, NY, USA: Springer-Verlag, 1989.
[6] M. Brokate and J. Sprekels, *Hysteresis and Phase Transitions*. New York, NY, USA: Springer-Verlag, 1996.
[7] A. Adly, I. Mayergoyz, and A. Bergqvist, "Preisach modeling of magnetostrictive hysteresis," *J. Appl. Phys.*, vol. 69, no. 8, pp. 5777–5779, 1991.
[8] A. Cavallo, C. Natale, S. Pirozzi, and C. Visone, "Effects of hysteresis compensation in feedback control systems," *IEEE Trans. Magn.*, vol. 39, no. 3, pp. 1389–1392, May 2003.
[9] M. A. Janaideh, S. Rakheja, and C.-Y. Su, "An analytical generalized Prandtl–Ishlinskii model inversion for hysteresis compensation in micropositioning control," *IEEE/ASME Trans. Mechatronics*, vol. 16, no. 4, pp. 734–744, Aug. 2011.
[10] K. Kuhnen, "Modeling, identification and compensation of complex hysteretic nonlinearities: A modified Prandtl–Ishlinskii approach," *Eur. J. Control*, vol. 9, no. 4, pp. 407–418, 2003.
[11] X. Tan and H. K. Khalil, "Two-time-scale averaging of systems involving operators and its application to adaptive control of hysteretic systems," in *Proc. Amer. Control Conf.*, Jun. 2009, pp. 4476–4481.
[12] K. Kuhnen and H. Janocha, "Adaptive inverse control of piezoelectric actuators with hysteresis operator," in *Proc. Eur. Control Conf.*, Karsruhe, Germany, 1999, no. F0291.

[13] S. Valadkhan, K. Morris, and A. Khajepour, "Robust PI control of hysteretic systems," in *Proc. 47th IEEE Conf. Decision Control*, Dec. 2008, pp. 3787–3792.
[14] A. Esbrook, X. Tan, and H. K. Khalil, "Control of systems with hysteresis via servocompensation and its application to nanopositioning," *IEEE Trans. Control Syst. Technol.*, vol. 21, no. 3, pp. 725–738, May 2013.
[15] X. Tan and J. S. Baras, "Modeling and control of hysteresis in magnetostrictive actuators," *Automatica*, vol. 40, no. 9, pp. 1469–1480, 2004.
[16] Q. Xu and Y. Li, "Radial basis function neural network control of an XY micropositioning stage without exact dynamic model," in *Proc. IEEE/ASME Int. Conf. Adv. Intell. Mechatron.*, Jul. 2009, pp. 498–503.
[17] J. Shen, W. Jywea, H. Chiang, and Y. Shub, "Precision tracking control of a piezoelectric-actuated system," *Precis. Eng.*, vol. 32, no. 2, pp. 71–78, 2008.
[18] S. Bashash and N. Jalili, "Robust multiple frequency trajectory tracking control of piezoelectrically driven micro/nanopositioning systems," *IEEE Trans. Control Syst. Technol.*, vol. 15, no. 5, pp. 867–878, Sep. 2007.
[19] H. Liaw, B. Shirinzadeh, and J. Smith, "Enhanced sliding mode motion tracking control of piezoelectric actuators," *Sens. Actuators A, Phys.*, vol. 138, no. 1, pp. 194–202, 2007.
[20] C. Jan and C. Hwang, "A nonlinear observer-based sliding-mode control for piezoelectric actuator systems: Theory and experiments," *J. Chin. Inst. Eng.*, vol. 27, no. 1, pp. 9–22, 2004.
[21] G. Schitter, A. Stemmer, and F. Allgöwer, "Robust two-degree-of-freedom control of an atomic force microscope," *Asian J. Control*, vol. 6, no. 2, pp. 156–163, 2004.
[22] Y. Wu and Q. Zou, "Robust inversion-based 2-DOF control design for output tracking: Piezoelectric-actuator example," *IEEE Trans. Control Syst. Technol.*, vol. 17, no. 5, pp. 1069–1082, Sep. 2009.
[23] A. Sebastian and S. Salapaka, "Robust broadband nanopositioning: Fundamental trade-offs, analysis, and design in a two-degree-of-freedom control framework," *Nanotechnology*, vol. 20, no. 3, p. 035501, 2009.
[24] J. Zhong and B. Yao, "Adaptive robust precision motion control of a piezoelectric positioning stage," *IEEE Trans. Control Syst. Technol.*, vol. 16, no. 5, pp. 1039–1046, Sep. 2008.
[25] C. Y. Su, Y. Stepanenko, J. Svoboda, and T. P. Leung, "Robust adaptive control of a class of nonlinear systems with unknown backlash-like hysteresis," *IEEE Trans. Autom. Control*, vol. 45, no. 12, pp. 2427–2432, Dec. 2000.
[26] S. Bashash and N. Jalili, "Robust adaptive control of coupled parallel piezo-flexural nanopositioning stages," *IEEE/ASME Trans. Mechatronics*, vol. 14, no. 1, pp. 11–20, Feb. 2009.
[27] V. Utkin, J. Guldner, and J. Shi, *Sliding Mode Control in Electromechanical Systems*. New York, NY, USA: Taylor & Francis, 1999.
[28] C. V. Newcomb and I. Flinn, "Improving the linearity of piezoelectric ceramic actuators," *Electron. Lett.*, vol. 18, no. 11, pp. 442–443, 1982.
[29] A. J. F. B. Bhikkaji, M. Ratnam, and S. O. R. Moheimani, "High-performance control of piezoelectric tube scanners," *Electron. Lett.*, vol. 15, no. 5, pp. 853–866, 2007.
[30] M. Edardar, X. Tan, and H. K. Khalil, "Sliding-mode tracking control of piezo-actuated nanopositioners," in *Proc. Amer. Control Conf.*, 2012, pp. 3825–3830.
[31] K. Kuhnen and H. Janocha, "Inverse feedforward controller for complex hysteretic nonlinearities in smart-material systems," *Control Intell. Syst.*, vol. 29, no. 3, pp. 74–83, 2001.
[32] R. Iyer and X. Tan, "Control of hysteretic systems through inverse compensation," *IEEE Control Syst. Mag.*, vol. 29, no. 1, pp. 83–99, Feb. 2009.
[33] H. Khalil, *Nonlinear Systems*. Englewood Cliffs, NJ, USA: Prentice-Hall, 2002.
[34] P. Kokotovic, H. K. Khalil, and J. O'Reilly, *Singular Perturbation Methods in Control Analysis*. Philadelphia, PA, USA: SIAM, 1999.
[35] P. Ge and M. Jouaneh, "Tracking control of a piezoceramic actuator," *IEEE Trans. Control Syst. Technol.*, vol. 4, no. 3, pp. 209–216, May 1996.
[36] M. Edardar, X. Tan, and H. K. Khalil, "Closed-loop analysis for systems with fast linear dynamics preceded by hysteresis," in *Proc. Amer. Control Conf.*, Jun. 2013, pp. 3579–3584.
[37] M. Edardar, X. Tan, and H. K. Khalil, "Tracking error analysis for feedback systems with hysteresis inversion and fast linear dynamics," *J. Dyn. Syst., Meas. Control*, vol. 136, no. 4, p. 041010, 2014.

Mohamed Edardar received the B.S. degree from Tripoli University, Tripoli, Libya, in 1991, the M.S. degree from University Putra Malaysia, Darul Ehsan, Malaysia, in 1999, and the Ph.D. degree from Michigan State University, East Lansing, MI, USA, in 2013.

He is currently a member of the academic staff with the Department of Electrical and Electronic Engineering, Tripoli University. He has authored and peer-reviewed several papers. His current research interests include the analysis and design of control systems that involves hysteresis, and the modeling of systems using smart materials such as piezoactuators.

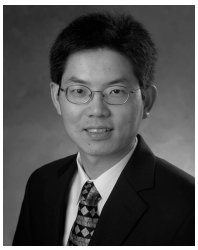

Xiaobo Tan (S'97–M'02–SM'11) received the B.Eng. and M.Eng. degrees in automatic control from Tsinghua University, Beijing, China, in 1995 and 1998, respectively, and the Ph.D. degree in electrical and computer engineering from the University of Maryland, College Park, MD, USA, in 2002.

He was a Research Associate with the Institute for Systems Research, University of Maryland, from 2002 to 2004. He joined the faculty of the Department of Electrical and Computer Engineering at Michigan State University (MSU), East Lansing, MI, USA, in 2004, where he is currently an Associate Professor. Since 2009, he has been leading an NSF-Funded Research Experiences for Teachers program at MSU. He has authored and co-authored one book (*Biomimetic Robotic Artificial Muscles*) and over 150 peer-reviewed journal and conference papers, and holds one U.S. patent. His current research interests include electroactive polymer sensors and actuators, modeling and control of smart materials, biomimetic robotic fish, mobile sensing in aquatic environments, and collaborative control of autonomous systems.

Dr. Tan serves on the editorial boards of *Automatica*, the IEEE/ASME TRANSACTIONS ON MECHATRONICS, and *International Journal of Advanced Robotic Systems*. He served as the Program Chair of the 2011 International Conference on Advanced Robotics, and is currently serving as the Finance Chair of the 2015 American Control Conference, the Chair of the ASME DSCD Technical Committee on Mechatronics, and the Liaison of the IEEE Control Systems Society to the IEEE Nanotechnology Council. He was a recipient of the NSF CAREER Award in 2006, the MSU Teacher-Scholar Award in 2010, and several Best Paper Awards.

Hassan K. Khalil (F'89) received the B.S. and M.S. degrees from Cairo University, Giza, Egypt, and the Ph.D. degree from the University of Illinois at Urbana-Champaign, Champaign, IL, USA.

He is a University Distinguished Professor of Electrical Engineering with Michigan State University, East Lansing, MI, USA. He consulted for General Motors and Delco Products, and published several papers on singular perturbations and nonlinear control. He has authored *Nonlinear Control* (2015), *Nonlinear Systems–3rd Edition* (2002), and has co-authored *Singular Perturbation Methods in Control: Analysis and Design–2nd Edition* (1999).

Prof. Khalil is a fellow of the International Federation of Automatic Control. He served as an Associate Editor of the IEEE TRANSACTIONS ON AUTOMATIC CONTROL, *Automatica*, and *Neural Networks*, and an Editor of *Automatica*. He was the Program Chair of the 1988 ACC and General Chair of the 1994 ACC. He was a recipient of the IEEE-CSS George Axelby Outstanding Paper Award, the AACC Ragazzini Education Award, the IFAC Control Engineering Textbook Prize, the AACC Hugo Schuck Best Paper Award, and the AGEP Faculty Mentor of the Year Award.